

Experimental and Numerical Study of Ballistic Impact Performance on Steel Plate Structures

Muhanad Hamed Mosa^{1*} , Ali Muslem Abed² , Salah M. Ali Al-Obaidi³ 

^{1,2}Department of Mechanical Engineering, College of Engineering, University of Al-Qadisiyah, Al-Diwaniyah, Iraq

³Institute of Noise and Vibration, University Teknologi Malaysia, Kuala Lumpur, Malaysia

*Email: muhanad.mosa@qu.edu.iq

Article Info

Received 15/06/2024

Revised 06/07/2024

Accepted 06/07/2024

Abstract

High-strength steel plates are commonly employed in civil and military vehicles to provide ballistic protection against various threat levels. This work's experimental tests involved shooting a 2 mm steel target (150×150 mm) with a Parabellum 9 × 19 full metal jacket projectile moving at a ballistic velocity of 370 m/s. On the other hand, numerical work was conducted to simulate the same event using LS-DYNA, an explicit finite element code. This work aimed to demonstrate the capability of LS-DYNA software in simulating the effects of ballistic impact and analyzing the performance of steel plate armor. The numerical analysis showed that all constitutive relations effectively predicted the qualitative behavior of the physical mechanisms during perforation. The influence of fracture criteria on numerical simulations of the perforation process was investigated. Detailed discussions were provided regarding the reasons behind these findings. For practical applications, the suitable selection of the type of constitutive model and criterion of fracture employing the finite element method (FEM) leads to an excellent agreement with the experimental results of projectile impacts on steel targets under the same conditions.

Keywords: Armor Perforation; Ballistic Impact; Finite Element Method; Johnson-Cook model; LS-DYNA

1. Introduction

Perforation of any target by bullets involves various parameters such as strain and strain rate hardening, elastic and plastic deformation, plugging, crack formation, pedaling failure, shearing, and even thermal softening [1],[2]. These parameters depend on the characteristics and geometry of both the panels and projectiles and impact velocity. The first significant challenge is the complexity of experimental analysis, which demands advanced tools and laboratory facilities. Consequently, the numerical method is often the most reliable choice [3]; on the other hand, the second issue is selecting the appropriate FEM software for the specific case being studied. [4]-[6]. Comprehensive experimental and theoretical implementation in this scope has been documented [6]-[8]. Specific studies have investigated phenomena such as shear plugging and petalling failure in thin metallic plates [9],[10]. Additional work has focused on the effects of plate thickness and projectile shape [1]-[11]. The Finite Element Method (FEM) has been extensively used to simulate ballistic impact events [12],[13], highlighting its significance. The objective of this work is to compare the compatibility of both experimental and numerical approaches using LS-DYNA software. In the

experimental part, 9 mm FMJ projectiles with a velocity of 370 m/s are used to penetrate 2 mm thin steel plates. Conversely, the numerical simulation of the ballistic test is conducted in the second part. Furthermore, test data, including residual velocity, energy absorption, and failure modes, are compared with numerical simulation results in the final section of this article. The importance and contribution of the work are represented in a detailed comparison between experimental and numerical works using important software such as LS-Dyna software. It is considered one of the most important software in this field but is not widely used. Hence, one of the foundations of this work is to highlight the software's ability to find many solutions for many complicated studies in the ballistic impact field.

2. Materials and Test

2.1. Target Properties

Square panels measuring 150×150 mm were made from (steel-1080) with a thickness of 2mm and were used in the experimental part of this work. The plate's thermal Conductivity and Specific Heat are 47.7 W/m-K and 0.490 J/g-°C, respectively. Capacity to guarantee precise determination of the mechanical properties of steel plates, a tensile test was

considered using a universal testing machine. Test specimens were prepared according to ASTM standard E8/E8M using a water jet machine to achieve smoothness and mitigate the potential stress concentration resulting from the non-uniform shapes due to the cutting of specimens. Fig. 1 shows the appearance of the steel panel with the steel specimen subject to the tensile test beside the stress-strain curve. Table 1 also provides the essential elastic and plastic parameters.

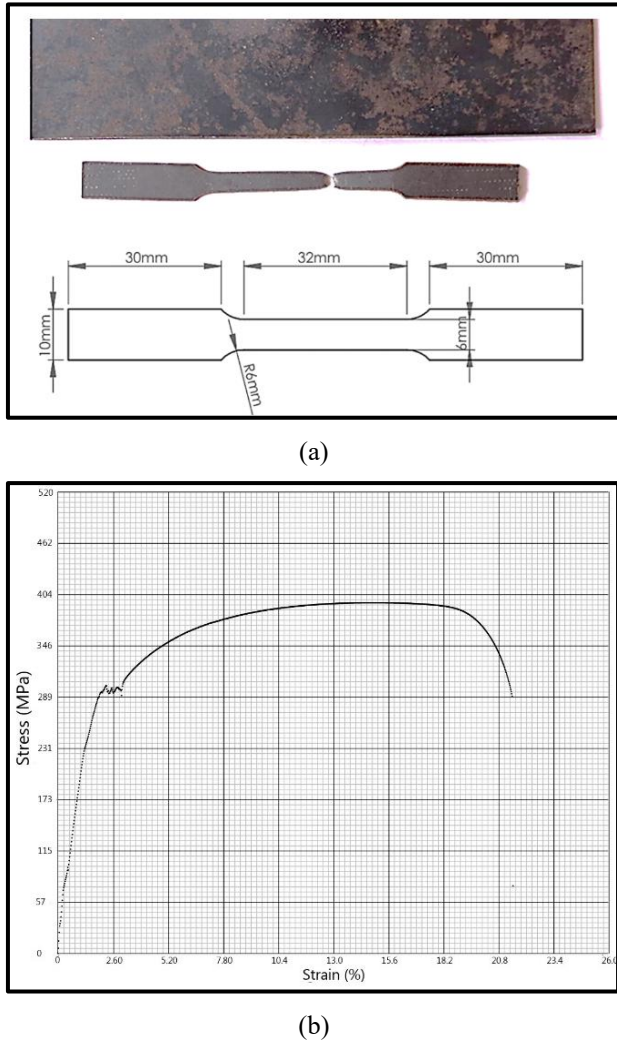


Figure 1. The steel plates and specimen after the tensile test with dimensions of specimens also, the stress-strain curve

Table 1. Mechanical properties of steel plate-1080

Material	E (GPa)	G (GPa)	ν	σ_{UL} (MPa)	ρ (kg/m ³)
Steel-1080	202.7	79.8	0.28	392	7706

2.2. Nine mm Bullet Properties

Bullet properties comprise various critical properties that affect its functionality and performance. Among these are hardness and elasticity, vital for maintaining the forces that stand up during a ballistic impact [14]. The composition of the material,

typically lead encased inside a copper jacket, significantly influences the bullet behavior. Moreover, dimensions such as length and radius affect stability and penetration strength. Additionally, mass distribution and geometry influence path and terminal ballistic impact performance. Specifications of a 9mm FMJ, also known as 9x19mm Parabellum, include several definitive aspects. The mass of the bullet is 8.5 grams, and it features a full metal jacket (FMJ). The bullet's length without the cartridge is 15 mm. Fig. 2 illustrates the appearance of the 9 mm bullet.

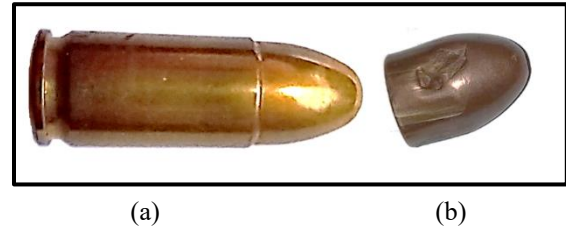


Figure 2. Nine mm bullet photo (a) With cartridge (b) Without cartridge

It's crucial to know that while these specifications offer a broad spectacle, variations can occur among industrialists and specific ammunition loads. Hence, referencing the exact details provided by manufacturers is essential for precise understanding and analysis. Table 2 lists the mechanical characteristics of the bullet's core materials and jacket, comprising lead and brass, respectively [11].

Table 2. Mechanical properties of 9 mm bullet [4]

Part	Modulus of Elasticity (GPa)	Tangent Modulus (GPa)	Poisson Ratio	Density (kg/m ³)
Jacket	116	506	0.32	8503
Core	16.5	14	0.41	11262

2.3 Experimental Work

The work adopted the National Institute of Justice (NIJ) as the standard reference for conducting ballistic impact tests to assess specimen performance. Notably, many institutions, such as the Home Office Scientific Development Branch (HOSDB) and the North Atlantic Treaty Organization (NATO) [15]. However, the NIJ standards were particularly selected due to their common recognition and approval within the area, attributed to their universal guidelines and severe testing protocols. By following the NIJ standards, the work endeavors to ensure solidarity and comparability in evaluating the ballistic performance of the specimens under realization [15].

In the ballistic impact experiment, two fundamental kinds of penetration are observed: partial and complete penetration. Complete penetration takes place while the bullet fully crosses the panel; on the other hand, partial penetration includes only partial entry into the panel. In ballistic impact experiments, full penetration is particularly useful for assessing the energy absorption by the panel or the lost energy by the bullet upon

test. Usually, this test is achieved experimentally by utilizing two chronographs, which are used to measure the speed of the projectile before and after the ballistic impact. Fig. 3 offers a chronograph device, the tool used to fix the specimens before the ballistic test.



Figure 3. Ballistic test equipment:(a) Chronographs, (b) Specimen fixing tool

The strike or initial velocity of bullets represents the speed before the impact, besides the velocity after penetration, called the residual velocity. Fig. 4 shows the arrangement of the device in the ballistic impact test. However, the following equation calculates lost or absorbed energy via a bullet and panel. However, Equation (1) is used to describe LEB (the lost energy of the bullet (J)), m_b is the mass of the bullet, and V_i and V_r are the initial and residual velocities (m/sec), respectively [16].

$$LEB = 0.5 \times m_b \times (V_i^2 - V_r^2) \tag{1}$$

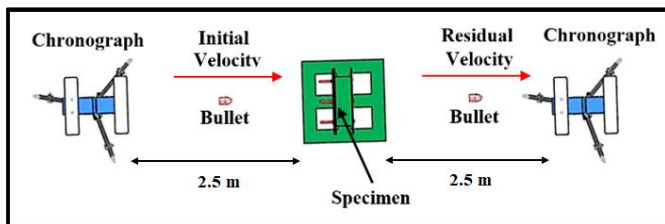


Figure 4. Schematic showing the top view of the ballistic test equipment and bullet path according to NIJ standard

3. Finite Element Modeling

3.1 Mesh Generation

LS-DYNA is a common software that uses the finite element method to analyze the body's response to static and dynamic loads. A 9 mm FMJ bullet consists of two major parts: the jacket and core. The jacket is made of brass material, covering the bullet's outer surface with a 0.4 mm thickness. On the other side, the material of the core is lead and represents the fatal part of the bullet. A 3D hexahedron mesh was utilized to model this projectile, as depicted in Fig. 5.

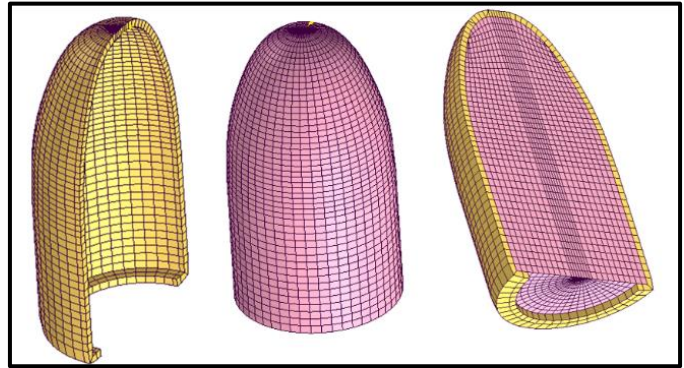


Figure 5. Nine mm FMJ bullet model After mesh generation

To create the mesh employing LS-DYNA, the process includes initially utilizing the tool 2D Mesh Generation to create a quadrilateral mesh, then a 3D mesh by revolving the previous 2D mesh about the axis of the edge, hence creating a hexahedron shape of mesh for the jacket and core. The total number of nodes and elements in the core and jacket is listed in Table 3.

Table 3. Number of Elements and Nodes For a 9 mm bullet

Type	Elements Numbers	Nodes Numbers
Jacket	5402	2700
Core	29200	29843

To define the mesh for the plate, a 3D mesh was employed (hexahedron mesh) to mesh the target of the steel panel; the fundamental tool used for this purpose is the Box Solid tool to create the plate's simple structure (3D quadrilateral mesh). The process includes choosing the elements in each direction (X-Y-Z) to build this model. Boundary condition was specified to simulate the clamping conditions (The steel plate is fixed on all edges) with two layers. The dynamic friction coefficient of 0.65 is typical for clean dry. The elements and nodes for the target are provided in Table 4. Also, Fig.6 offers the hexahedron mesh for the target.

Table 4: Number of Elements and Nodes for steel plate

Type	Elements Numbers	Nodes Numbers
Steel	160,000	202,005

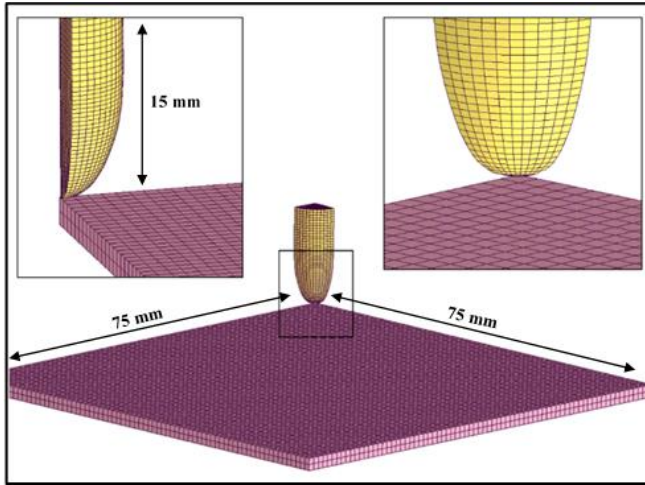


Figure 6. Steel plate model (Quarter of plate) with bullet after 3D mesh generation

3.2 Mathematical Models

Due to its simplicity, the Johnson-Cook (JC) empirical model is extensively utilized today, particularly for metallic materials. This model independently accounts for strain rate and temperature effects on flow stress. Therefore, when analyzing any structure, it is crucial to consider a range of temperatures and deformations. Equation (2) is used to express this model as follows [17]:

$$\sigma_y = (a + b\bar{\epsilon}^n)(1 + c \ln \dot{\epsilon})(1 - T^m) \quad (2)$$

σ_y is flow stress (MPa), and the parameters a , b , c , and n are constants (466, 338, 0.031, and 0.71, respectively) that represent the yield stress of the material under reference deformation conditions (MPa), Strain hardening constant (MPa), Strain rate strengthening coefficient, and Strain hardening coefficient respectively. Also, $\dot{\epsilon}$ effective plastic strain rate [18].

$$T^m = \frac{T - T_{room}}{T_{room} - T_{melt}} \quad (3)$$

T^m can be found by using Equation (3), T , T_{room} , and T_{melt} , which are Homologous temperature (K), Deformation temperature (K), Reference deformation temperature (K), and Melting temperature of the material, respectively. However, the melting temperature is about 1452 C, and m is 7006. The fracture occurs when the value of D equals one, as shown in Equation (4). However, the fracture parameters of the Johnson-Cook mode (D_1 , D_2 , D_3 , D_4 , and D_5) are (0.026, 16.89, -14.77, 0.0213, and 0.001, respectively) [11].

$$D = \sum \frac{\Delta \epsilon^{-p}}{e^f} \quad (4)$$

Moreover, the Cowper–Symonds model employs a straightforward empirical formulation to characterize strain rate hardening and strain. This model can determine the initial yield stress by considering both strain rate and strain. This formulation is essential for understanding the material behavior; all terms must be derived from experimental approaches. The mathematical expression of this model is indicated by using Equations (5) and (6) as follows [19]:

$$S_y = \left[1 + \left(\frac{\dot{\epsilon}}{C} \right)^{1/p} (S_o + \beta E_p \epsilon_p^{eff}) \right] \quad (5)$$

$$E_p = \frac{E_{tan} - E}{E - E_{tan}} \quad (6)$$

Therefore, the effectiveness of this material model largely relies on the data obtained from experimental tests. Additionally, the accuracy of any model's description is influenced by the constant values and the type of model chosen. Consequently, the Cowper–Symonds constitutive model has been validated for its capability to assess various structures subjected to high strain rates. [20].

4. Results and Discussion

4.1 Residual Velocity of Experimental and Theoretical Results.

This work employs two types of constitutive models to model both the projectile and targets. Thus, the validation process is definitive to ensure the reliability and precision of the numerical modeling. This work concentrates on assessing the performance of targets after ballistic impact by a 9mm FMJ bullet. The projectiles' velocity after impact (residual velocity) was employed to validate the numerical simulation results. Table 5 shows the initial and residual velocities after the experimental and numerical works. In this context, the table explains a strong agreement between these approaches, with an error percentage equal to 5.2 % and 9.3 % for the residual velocity and the lost energy of the bullet, respectively.

Table 5: Initial and residual velocity results in both experimental and numerical approaches

Steel plate	Experimental	Numerical	Error %
Initial velocity (m/s)	370	370	0
Residual velocity (m/s)	253	266	5.2
LEB (J)	255	232	9.3

The projectile's kinetic energy benefits the energy the structure must absorb after ballistic impact. Fig. 7 demonstrates the history of the bullet velocity during the ballistic impact with samples of plate deformation. Thus, from this figure, this work observed that the ballistic velocity gradually decreases from

370 m/s to 266 m/s within 75 μ sec, and the reason for this decrease is the conversion of energy from kinetic energy to strain energy as distortion in the plate. Consequently, it depends on the failure the panel has been exposed to.

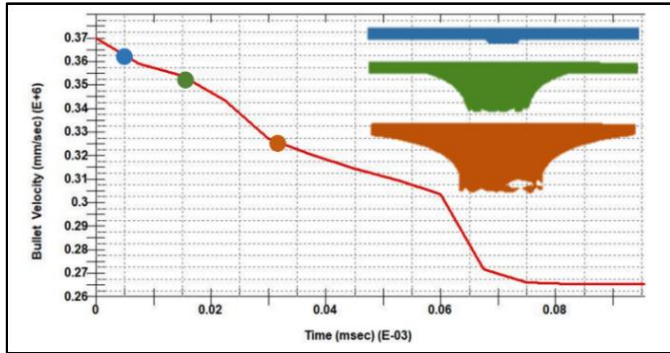


Figure 7. History of the bullet velocity compared with the amount of kinetic energy

4.2 Energy Absorption, Fracture, and Plate Distortion

The response of a target to the ballistic impact can vary depending on huge factors, including the characteristics of the target, the impact angle, and the projectile's mass and velocity; usually, in the region of the impact, the target submitted to the rapid deformation in a short time. This deformation can be apparent as elastic with plastic failure (permanent deformation) because the impacted zone directly impacted by the projectile will cause localized damage with the high energy transmitted from the projectile to the target. The structure of the target, such as the thickness and composition of the panel, also plays a vital role in the fracture type.

However, due to the high stresses in the impact area, cracks may propagate from the local region to the nearby area. Fig. 8 explains the gradual stress transition in a very short time (32 μ sec).

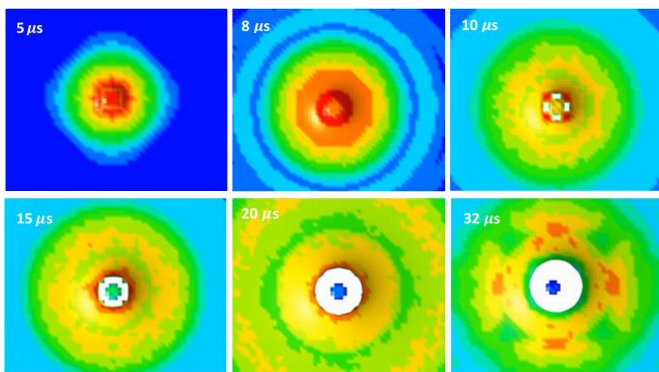


Figure 8. The surface stress field shows the front face of the steel plate after the ballistic impact and the time of effects.

As seen from Fig. 8, initially, when the bullet makes contact with the plate, the stress is concentrated in the local zone (around the site of impact). This localized stress gradually spreads from the inside to the outside area. Hence, the stress distribution develops in a short time and spreads through the target structure. Thus, the stress levels will increase rapidly and propagate as the distortion through the steel structure. However, Spalling or fragmentation is often observed in this event, especially at high impact speed; in this work, spalling appeared after 15 μ sec due to high energy absorption.

The form of deformation over short sectors of time (5, 8, 15, 20, and 32 μ sec) witnesses a significant change, and this depends mainly on the material's ability to deform, especially the ductility property, which is considered one of the distinctive properties of metallic materials. Thus, on the opposite side of the steel panel (back face), the deformation of the steel plate increases clearly and rises directly during the energy transmission. Fig.9 illustrates the stress distribution within the steel plate during the impact event.

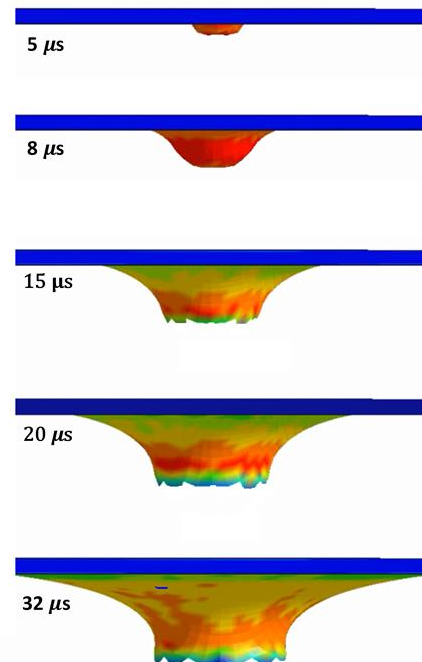


Figure 9. Historic deformation of the rear side of the steel plate

The kinetic energy of the projectile leads to distortion of the steel panel. Besides, it transforms into heat and occasionally spalls. Failure, petaling plugging, and fragmentation failure. Fig. 10 compares experimental and numerical betaling failure in the steel plate.

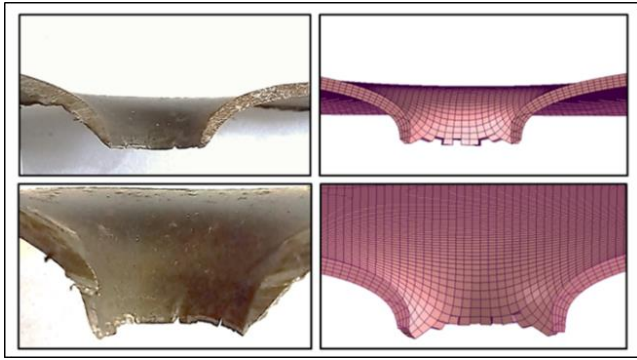


Figure 10. Comparison between experimental and numerical petaling deformation of steel plate after impact

Thus, the present work validated the mode of failure to guarantee the accuracy of the numerical model of the ballistic impact compared to the experimental test. However, the steel plate is isotropic, which means the characteristics in all directions are the same. Therefore, the most likely failure mode of the steel plate is petaling deformation.

The comparative analysis detects several keys that can be observed regarding the deformation behavior of the target in numerical simulation versus experimental tests. Both approaches explain a similar overall deformation response, including bending, bulging, or stretching. On the other hand, numerical simulations supply additional data about the internal stress distribution and localization of strain. Hence, they may not be readily observable in experimental testing. Also, numerical simulations permit parametric studies to discuss the influence of various factors on the panel's behavior after impact. Fig. 11 offers a more inclusive comparison between the two approaches to understanding the underlying mechanisms.

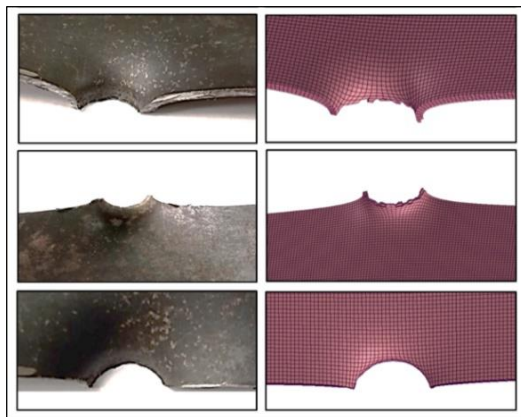


Figure 11. Longitudinal section of the deformation after ballistic impact of steel plate in the experimental and numerical approaches

5. Conclusions

From the present work, experimental analysis and numerical simulation have been achieved, and thin steel plates (2 mm) were subjected to ballistic impact by a 9 mm bullet with an incident velocity of 370 m/sec. The lost energy from the projectile was calculated experimentally and numerically by

measuring the initial and residual velocities. Numerical simulations were conducted using the Explicit LS-DYNA code, incorporating the Johnson and Cook plasticity algorithm with a strain rate with fracture criterion, to reproduce the experimental tests. The results show agreement between the predicted numerical work and the experimental approach. However, the energy absorbed predicted by the simulation work closely matches with the experimental test.

On the other hand, the numerical model successfully apprehends transference in modes of failure. Furthermore, work was conducted on the strain rates during deformation within the specimens under ballistic impact. Finally, this work confirms the significance of both experimental analysis and numerical simulation approaches to understanding the behavior of steel plates under ballistic impact. The close agreement between experimental and predicted data highlights the effectiveness of the utilized numerical method. It emphasizes the importance of the reliability of LS-DYNA software in this scope of work.

Acknowledgments

The authors would like to express our gratitude to Al-Qadisiyah University/ College of Engineering for providing the necessary equipment to complete the work.

Conflict of interest

The authors declare that there are no conflicts of interest regarding the publication of this manuscript.

Author Contribution Statement

Muhanad Hamed Mosa conducted the simulation work and analysis of the results.

Ali Muslem Abed stated the the problem statement and analyzed the theory according to analytical methods.

Salah M. Ali Al-Obaidi proposed the work.

Symbols		
a	Constant represents the yield stress	MPa
b	Strain hardening constant	MPa
c	Strain rate strengthening coefficient	MPa
D	Damage parameter	-
E	Elastic modulus	MPa
E _p	Plastic hardening modulus	MPa
E _{tan}	Tangent elastic modulus	MPa
G	Modulus of rigidity	Gpa
LEB	The lost energy of the bullet	J
m _b	Mass of the bullet	kg
n	Strain hardening coefficient	MPa
T ^m	Homologous temperature	K

T_{room}	Reference deformation temperature	K
T_{melt}	Melting temperature of the material	K
T	Deformation temperature	K
v_i	Initial velocity	m/s
v_r	Residual velocity	m/s
σ_y	Flow stress	MPa
ϵ	Effective plastic strain rate	s ⁻¹
ν	Poisons' ratio	-
e^f	Strain at fracture	-
S_y	Shear strength	MPa
S_y	Cowper–Symonds strain rate	MPa
β	Strain hardening parameter	-
ϵ^{peff}	Effective plastic strain	-
σ_{ul}	Ultimate strength	MPa
ρ	Density of material	Kg/ m ³

References

- [1] M. Naik, Pranay, V, Thakur, DG, Chandel, Sunil, Salunkhe, Sachin, Pagac, Marek, Abouel Nasr, Emad S "Numerical investigation on effect of different projectile nose shapes on ballistic impact of additively manufactured AlSi10Mg alloy," *Frontiers in Materials*, vol. 11, p. 1330597, 2024. <https://doi.org/10.3389/fmats.2024.1330597>
- [2] P. Fernando, Mohotti, Damith, Remennikov, Alex, Hazell, PJ, Wang, H, Amin, Ali "Experimental, numerical and analytical study on the shock wave propagation through impedance-graded multi-metallic systems," *International Journal of Mechanical Sciences*, vol. 178, p. 105621, 2020. <https://doi.org/10.1016/j.ijmecsci.2020.105621>
- [3] A. M. Petrucci, Vahedi, Khodadad, Rahmani, Masoud, Petrucci, MohammadAli Moslemi "Numerical and analytical simulation of ballistic projectile penetration due to high velocity impact on ceramic target," *Frattura ed Integrità Strutturale*, vol. 14, no. 54, pp. 226-248, 2020. <https://doi.org/10.3221/IGF-ESIS.54.17>
- [4] E. Palta, Fang, Hongbing, Weggel, David C "Finite element analysis of the Advanced Combat Helmet under various ballistic impacts," *International Journal of Impact Engineering*, vol. 112, pp. 125-143, 2018. <https://doi.org/10.1016/j.ijimpeng.2017.10.010>
- [5] M. Mosa, Fahem, Ali, Guthai, Achyuth Thumbalam "Experimental investigation of perforated multi-layered composite armor subjected to ballistic impact," *Al-Qadisiyah Journal for Engineering Sciences*, vol. 17, no. 1, pp. 16-21, 2024. <https://doi.org/10.30772/qjes.2024.146005.1083>
- [6] L. Peterson, Horstemeyer, Mark, Lacy, Thomas, Moser, Robert "Using an Internal State Variable Model Framework to Investigate the Influence of Microstructure and Mechanical Properties on Ballistic Performance of Steel Alloys," *Metals*, vol. 13, no. 7, p. 1285, 2023. <https://doi.org/10.3390/met13071285>
- [7] J. Pinkos, Stempien, Zbigniew, Małkowska, Magdalena "Numerical and experimental analysis of ballistic performance in hybrid soft armours composed of para-aramid triaxial and biaxial woven fabrics," *AUTEX Research Journal*, vol. 24, no. 1, p. 20230022, 2024. <https://doi.org/10.1515/aut-2023-0022>
- [8] Z. Gao, Chen, Yeqing, Wang, Zhenqing, Li, Shutao, Wei, Wanli, Chen, Jialin "Shattering Effect Study of Aramid–Steel Composite Target Plates under Localized Blast Loading," *Sustainability*, vol. 15, no. 5, p. 4160, 2023. <https://doi.org/10.3390/su15054160>
- [9] M. H. Mosa, Hamza, Mohsin Noori, "Influence of selection materials and construction techniques on the ballistic performance of armors: A review," in *AIP Conference Proceedings*, 2021, vol. 2404, no. 1: AIP Publishing. <https://doi.org/10.1063/5.0068916>
- [10] B. Liu, Soares, C Guedes "Effect of strain rate on dynamic responses of laterally impacted steel plates," *International Journal of Mechanical Sciences*, vol. 160, pp. 307-317, 2019. <https://doi.org/10.1016/j.ijmecsci.2019.06.034>
- [11] J. K. Holmen, Hopperstad, Odd Sture, Børvik, Tore "Low-velocity impact on multi-layered dual-phase steel plates," *International Journal of Impact Engineering*, vol. 78, pp. 161-177, 2015. <https://doi.org/10.1016/j.ijimpeng.2014.12.005>
- [12] S. Choudhary, Singh, Pundan Kumar, Khare, Sangeeta, Kumar, Krishna, Mahajan, Puneet, Verma, Rahul Kumar "Ballistic impact behaviour of newly developed armour grade steel: an experimental and numerical study," *International Journal of Impact Engineering*, vol. 140, p. 103557, 2020. <https://doi.org/10.1016/j.ijimpeng.2020.103557>
- [13] R. Zhang, Qiang, Lu-Sheng, Han, Bin, Zhao, Zhen-Yu, Zhang, Qian-Cheng, Ni, Chang-Ye, Lu, Tian Jian "Ballistic performance of UHMWPE laminated plates and UHMWPE encapsulated aluminum structures: Numerical simulation," *Composite Structures*, vol. 252, p. 112686, 2020. <https://doi.org/10.1016/j.compstruct.2020.112686>
- [14] H. Tawfiq, Ghilaim, Kadhim H, Al-Hilli, Ali Hussain "Effects of hybrid arrangement and location of the stronger layer on the impact resistance of composite plate target," *Journal of Engineering and Sustainable Development*, vol. 13, no. 1, pp. 111-126, 2009. <https://jeasd.uomustansiriyah.edu.iq/index.php/jeasd/article/view/1538>
- [15] J. Black, Premo, Ryan, Goldberg, Robert K, Ricks, Trenton M, Lyons, Troy, Kim, Han-Gyu "Multi-Scale Experimental Characterization for LS-DYNA MAT213 Modeling of Composite Structures under High Strain Rate," *arXiv preprint arXiv:11316*, 2024. <https://doi.org/10.48550/arXiv.2403.11316>
- [16] A. Shokry, Gowid, Samer, Mulki, Hasan, Kharmanda, Ghais "On the prediction of the flow behavior of metals and alloys at a wide range of temperatures and strain rates using Johnson–Cook and modified Johnson–Cook-based models: a review," *Materials Today: Proceedings*, vol. 16, no. 4, p. 1574, 2023. <https://doi.org/10.3390/ma16041574>
- [17] V. K. R. Sirigiri, Gudiga, Vinith Yadav, Gattu, Uday Shankar, Suneesh, G, Buddaraju, Krishna Mohan "A review on Johnson Cook material model," *Materials Today: Proceedings*, vol. 62, pp. 3450-3456, 2022. <https://doi.org/10.1016/j.matpr.2022.04.279>
- [18] R. Rai, Kumar, Gaurav, Dagar, Sagar, Somashekar, V, Mboreha, Chanfiou Ahmed, Modi, Priyank "Numerical simulation of ballistic impact on aluminium 5083-H116 plate with Johnson cook plasticity model," *Materials Today: Proceedings*, vol. 46, pp. 10619-10627, 2021. <https://doi.org/10.1016/j.matpr.2021.01.373>
- [19] J. Dean, Dunleavy, CS, Brown, PM, Clyne, J, "Energy absorption during projectile perforation of thin steel plates and the kinetic energy of ejected fragments," *International Journal of impact engineering*, vol. 36, no. 10-11, pp. 1250-1258, 2009. <https://doi.org/10.1016/j.ijimpeng.2009.05.002>
- [20] D. Mohotti, Fernando, PLN, Weerasinghe, Dakshitha, Remennikov, Alex "Evaluation of effectiveness of polymer coatings in reducing blast-induced deformation of steel plates," *Defence Technology*, vol. 17, no. 6, pp. 1895-1904, 2021. <https://doi.org/10.1016/j.dt.2020.11.009>